Thermal annealing effects in polycrystalline $EuTiO_3$ and $Eu_2Ti_2O_7$

Juliana Schell,[1,2,a)] Stanislav Kamba,[3] Martin Kachlik,[4] Karel Maca,[4] Jan Drahokoupil,[3] B. Rahman Rano,[1,5] João Nuno Gonçalves,[6] Thien Thanh Dang,[7] Angelo Costa,[1] Cornelia Noll,[7] Reiner Vianden,[7] and Doru C. Lupascu[2]

[1]*European Organization for Nuclear Research (CERN), CH-1211 Geneva, Switzerland*
[2]*Institute for Materials Science and Center for Nanointegration, Duisburg-Essen (CENIDE), University of Duisburg-Essen, 45141 Essen, Germany*
[3]*Institute of Physics of the* Czech Academy of Sciences, *Na Slovance 2, 182 21 Prague 8, Czech Republic*
[4]*CEITEC—Central European Institute of Technology, Brno University of Technology, Purkyňova 123, 612 00 Brno, Czech Republic*
[5]*Department of Physics, University of Dhaka, Dhaka-1000, Bangladesh*
[6]*CICECO*—Aveiro Institute of Materials and Departamento de Física, *Universidade de Aveiro, 3810-193 Aveiro, Portugal*
[7]*Helmholtz-Institut für Strahlen- und Kernphysik, University of Bonn, 53115 Bonn, Germany*

ABSTRACT

Using time-differential perturbed angular correlation of γ rays, we investigated the electric-field gradient of polycrystalline $EuTiO_3$ and $Eu_2Ti_2O_7$, with $^{181}Hf(^{181}Ta)$ as a probe, following different thermal treatments. The measurements were performed at ISOLDE-CERN following 80 keV implantation at the Bonn Radioisotope Separator. The experimental results indicated successful induction of different phases in the implantation recovery process at 1273 and 1373 K. These observations were combined with *ab initio* calculations and X-ray diffraction measurements. A comparison of *ab-initio* calculated electric-field gradients with the measured values discriminates between different structures and defects and rules out many possible cases. The Ta probe at the Ti site in the $Eu_2Ti_2O_7$ phase is found to be the most probable case of site occupation after annealing at 1373 K, while annealing at 1273 K keeps $EuTiO_3$ in the vicinity of the Ta probe. A discussion of the hyperfine interactions which promote variation in the interaction strength at the ^{181}Ta site is presented.

Keywords: annealing effects, europium titanates, TDPAC, *ab initio* calculations, X-ray diffraction

a) Author to whom correspondence should be addressed. Electronic mail: juliana.schell@cern.ch, Tel: +41 75 411 7872

I. INTRODUCTION

The time-differential perturbed angular correlation (TDPAC) technique[1] has been recognized as an efficient local characterization technique in condensed matter research. In particular, TDPAC has been applied in investigations of hyperfine fields in perovskite-type titanates since the beginning of the 1970s,[2] allowing scientists to obtain remarkable results. For instance, the technique has been used to characterize phase transitions in ceramic samples of $PbTiO_3$ and $BaTiO_3$ by measuring the temperature dependence of the Ti-site electric-field gradients (EFGs) at temperatures very close to the ferroelectric-to-paraelectric transition temperature, T_c. The samples were doped with small amounts of Hf that emitted radiation from the $^{181}Hf(^{181}Ta)$ probe. The results showed that high-frequency nuclear quadrupole interactions decreased as the temperature approached T_c, clearly reflecting tetragonal-to-cubic transitions in both materials.[3] In addition, the polarization dependence of EFGs at different sites in $PbTiO_3$, $BaTiO_3$ and other oxides has been revealed by one *ab initio* study[4] and Landau theory for the relation between electric field and electric polarization,[5] which strongly support the usefulness of the TDPAC method.

In addition to the TDPAC method, the Mössbauer technique has also been used in the analysis of hyperfine parameters at Eu sites in $EuTiO_3$. The phase purity in bulk $EuTiO_3$ was investigated using ^{151}Eu-Mössbauer spectroscopy, between 90 K and 325 K. The extracted isomer shift for the major component was −12.45 mm/s, an isomer shift indicative of Eu^{2+} ; thus, the sample contained purely divalent Eu.[6] In thin $EuTiO_3$ films, a similar result was found.[7] The isomer shift has also been around –13 mm/s in other works.[8,9,10] The area ratio of the Eu^{2+} absorption relative to the total absorption, A_{Eu}^{2+}/A_{Eu}, was found to be 0.97 and the full width at half maximum of one component of the Lorentzian multiples was 2.92(4) mm/s.[8] $EuTiO_3$ is magnetically ordered below 5.5 K and shows a magnetic spectrum at 2.2 and 4.2 K. The extrapolated hyperfine field at 0 K is 325 ± 7 kOe. Oxygen-deficient perovskites, $EuTiO_x$, with x between 2.68 and 3, showed Mössbauer parameters which were identical to those of $EuTiO_3$. No indication of quadrupole splitting was noted.[9] Mössbauer spectroscopy is very useful because it easily distinguishes between the valence states through their different isomer shifts. The relatively small linewidth of the europium-151 Mössbauer transition facilitates the observation of two hyperfine interactions, the isomer shift and the magnetic hyperfine field. Observation of the third hyperfine interaction and the quadrupole interaction is more difficult.

Perovskite-type-titanate materials exhibit a rich variety of unusual and interesting ferroelectric, magnetic, and structural properties, and europium titanate ($Eu_{0.5}Ba_{0.5}TiO_3$) presents the specific functionalities required for a solid-state-based search for the permanent electric dipole moment of the electron.[11] For pure europium titanate the dielectric permittivity exhibits an unusually sharp decrease at the Néel temperature, T_N = 5.5 K, below which a G-type antiferromagnetic phase develops.[12] A high sensitivity of the permittivity to the magnetic order or to the magnetic field[12] is the signature of an extremely strong spin–phonon coupling in $EuTiO_3$, which allows ferroelectric and ferromagnetic phase transitions to be induced using epitaxial strain.[13] Magnetoelectric coupling is exceptionally high in the antiferromagnetic phase, although the crystal symmetry of $EuTiO_3$ forbids linear coupling, and only biquadratic magnetoelectric coupling has been observed.[14] Above room temperature (RT), $EuTiO_3$ crystallizes in the cubic $Pm\bar{3}m$ perovskite structure, but near 282 K it undergoes an antiferrodistortive structural phase transition to the tetragonal *I4/mcm* phase.[15-17] Defects such as oxygen vacancies and Eu^{3+} ions strongly influence the temperature of the phase transition from a cubic to a tetragonal structure.[16]

Pyrochlore-phase $Eu_2Ti_2O_7$ presents the Eu^{3+} configuration ($EuTiO_3$ contains Eu^{2+}), which is attractive due to its strong spin-orbit coupling and appreciable magnetic susceptibility;[18] it is an n-type semiconductor with an energy band gap of approximately 2.5 eV and can form in a nanocrystalline form, in which case it possesses two inequivalent positions for the Eu^{3+} ions (core and surface).[19] Additionally, titanium pentoxide (Ti_3O_5) is a functional material that has attracted much attention from researchers, finding use in several applications.[20]

The potential applications of perovskite $EuTiO_3$, and pyrochlore $Eu_2Ti_2O_7$, motivated this paper, in which we report the first TDPAC experiments on these compounds, supported by X-ray diffraction (XRD) and *ab initio* calculations.

The variety of unusual and interesting ferroelectric, magnetic, and structural properties in europium titanates require such local characterization for a deeper understanding of the Eu^{3+}/Eu^{2+} influence in applications.

II. MATERIALS AND METHODS

A. Processing of experimental samples

Bulk polycrystalline ceramic samples were prepared from a mixture of Eu_2O_3 (68.778 wt.%) and TiO_2 (anatase, 31.222 wt.%) powders, which were homogenized in a planetary ball

mill for 30 min (ZrO_2 milling balls and bowls). Disc-shaped green bodies (diameter 15 mm, thickness 5 mm) were formed by uniaxial pressing (40 MPa) followed by cold isostatic pressing (300 MPa). The samples were sintered in a pure (99.9%) hydrogen atmosphere with a gas flow of 5 l/min (pressure ca 1.05 bar); the sintering temperature was 1673 K, with a 2-h dwell time (the heating and cooling rates were 10 K/min). The resulting $EuTiO_3$ ceramics contained no secondary phases prior to further annealing. More details of the samples' processing are described elsewhere.[21]

HfO_2, with natural isotopic composition, was irradiated for 6 days by a thermal neutron flux of 10^{15} n.cm^{-2} s^{-1} in the high-flux reactor of the Institut Laue-Langevin (ILL) in Grenoble, in order to produce ^{181}Hf via the ^{180}Hf(n,γ) reaction. The nuclear probe ^{181}Hf was implanted in the samples at 80 keV at the Bonn Radioisotope Separator (BONIS).[23,23]

Following implantation, radiation damage was annealed in a vacuum in two steps: first, at 1273 K for 5 h, then at 1373 K for 5 h. TDPAC measurements were carried out at ISOLDE-CERN[24,25] using conventional and digital set ups.[26,27] Theoretical perturbation functions were fitted to the spectra using Nightmare software,[28] to extract hyperfine parameters.

TDPAC measurements were performed at 10 and 295 K, in order to investigate the static electric quadrupole interactions of ^{181}Hf(^{181}Ta) in $EuTiO_3$ and $Eu_2Ti_2O_7$. To our knowledge, no TDPAC measurements had been done before in either system.

Following the TDPAC experiments, the samples were measured in Bragg-Brentano geometry on a PANalytical X´Pert PRO diffractometer equipped with a Co tube (λ = 0.178901 nm).

B. Time-differential perturbed angular correlation (TDPAC) of γ-rays method

The TDPAC technique is a powerful tool for studying hyperfine fields in solids, one of its advantages being the possibility of obtaining information on lattice defects and charge fluctuations. The charge distribution at the ^{181}Hf(^{181}Ta) lattice site induces an EFG. Due to suitable nuclear properties and the relatively long half-life of the probe, it is possible to follow the evolution of phase transitions as a function of temperature, with high sensitivity. The TDPAC technique measures the perturbation function $R(t) \approx A_{22}G_{22}(t)$ for different perturbation factors $G_{22}(t)$.[29,30] Considering spin $I = 5/2$ and static electric quadrupole perturbations in the polycrystals, the theoretical expression (1) is valid for a non-axially symmetric EFG:

$$G_{22}(t) = s_0 + \sum_{n=1}^{3} s_n(\eta)\cos[\omega_n(\eta)t]. \quad (1)$$

The quantity t is the time spent in the intermediate state of gamma quantum emission. The transition frequencies, ω_n, are given by $\omega_n = [E(M) - E(M)]/\hbar = 3|M^2 - M'^2|\omega_Q$.[29] The coefficients, s_n, denote the amplitudes, which can be determined by diagonalization of the interaction Hamiltonian, as well as the transition frequencies.[31,32] Since the EFG is represented by a symmetrical and traceless (3 × 3) tensor, it can be fully characterized by the magnitude V_{zz} and the asymmetry parameter $\eta = (V_{xx} - V_{yy})/V_{zz}$; η varies from 0 to 1, where 1 is for maximal asymmetry. The transition frequencies are functions of the nuclear quadrupole frequency, which is defined by:

$$\omega_Q = \frac{eQV_{zz}}{4I(2I-1)\hbar}, \quad (2)$$

where Q is the nuclear quadrupole moment and I = 5/2. The fundamental observed frequency, ω_0, is the main hyperfine parameter considered in this work for reporting the experimental nuclear quadrupole interaction. The parameter δ accounts for the normal distribution of relative width around ω_0.

If there are probe atoms exposed to j different lattice environments, and each of them creates a characteristic EFG at fraction f of the probe atom sites, the perturbation function becomes $R(t) = A_{22}\sum_j f_j G_{22}^j(t)$. In our case, a two-site model for data analysis was considered.

The hyperfine interactions between the EFGs and nuclear quadrupole moment, Q, of the probe nuclei can be either dynamic or static. Dynamic interactions occur because of time-dependent oscillations in the anisotropic γ emission, which are caused by the random fluctuations of hyperfine fields with a short correlation time, τ. Such interactions have been observed in measurements performed with ^{111}In[33,34] or ^{181}Hf[35] and are particular to EFG changes in magnitude or orientation, resulting from a dynamic spin-relaxation during the lifetime of the intermediate state; the interactions have been quantified by the transition rate between two states.[36] An increase in this rate results in increasing exponential damping of the modulation amplitudes in the time spectrum. In contrast with the static case, an increase causes identical line broadening or damping for different ω_n frequencies in the Fourier transform,[37] and the R(t) spectrum can also be damped to 0. However, in the limit of very high transition rates, nuclear spin does not occur. Furthermore, the strength and orientation of the EFG are constant in time for static interactions.

For our data analysis, static quadrupole interactions were considered. Attenuation of the oscillation amplitudes for static interactions can be caused by randomly distributed defects around the probe. Damping of the frequency oscillations in time can be approximated by the Lorentzian or Gaussian distribution[38] of frequencies around a central value of ω_0. The full width at half maximum is $FWHM/2 = \delta\omega_0/100$, with δ in % or $FWHM = \delta\omega_0\sqrt{8ln2}$ for the Lorentzian and Gaussian distributions, respectively .[39] The experimental perturbation factor can be found in Ref. 40. Additional details about the TDPAC technique can be found in Refs. 30 and 31.

C. *Ab initio* calculations

We used the density functional theory PAW method[41] as implemented in the VASP code,[42] with the PBE functional,[43] to calculate the EFG of Ta at different lattice sites. We also used GGA + U, U = 5.7 and J = 1 eV for the Eu f electrons, following the work of previous researchers[44,45] who employed the approach of Dudarev *et al.* .[46]The atomic forces that appeared were minimized to values lower than 5–20 meV/Å (20 in some supercells). We used an energy cutoff of 520 eV (400 eV was used in some large supercells, which was sufficient for converged results according to several test calculations). Ferromagnetic ordering was considered (a few calculations with G-type antiferromagnetic (G-AFM) ordering showed very small differences in the EFG).

III. RESULTS AND DISCUSSION

Following the first thermal treatment, the Ta atoms are probably bound to random defects and interact with a very weak EFG, as can be observed in the spectra displayed in Fig. 1 (left), measured at 10 K and RT. As expected, randomly distributed defects around the probe did not lead to the measurement of a sharp frequency, but rather to a distribution of frequencies.

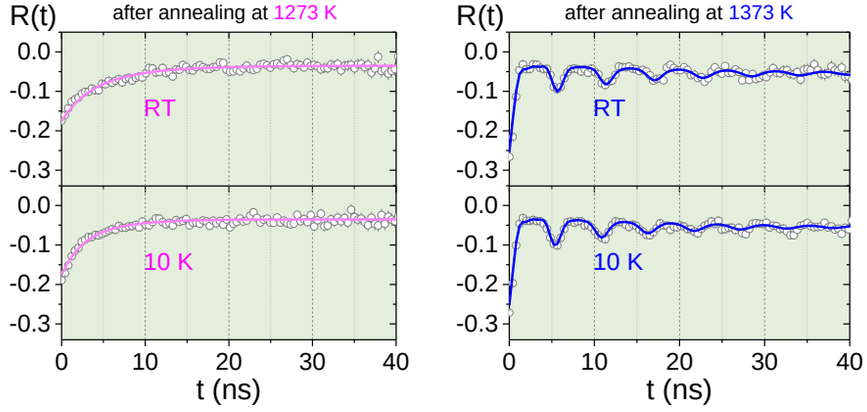

FIG. 1. Experimental *R(t)* functions measured at 10 K and RT after annealing at 1273 K (left) and 1373 K (right) using ^{181}Hf(^{181}Ta). The least-squares fits of the hyperfine parameters are represented by the pink and blue solid curves.

In order to fit the data shown in Fig. 1, we assumed a Lorentzian shape distribution for the EFG. For the $EuTiO_3$ phase, the very weak EFG distribution resulted from the cubic-symmetry deviation of the electric-charge distribution around Ta. For the measurements following annealing at 1273 K, we assumed a nuclear quadrupole interaction characterized by a distribution of frequencies with $<\omega_0>$ = 1 Mrad/s and FWHM =1.27(1) % at RT or FWHM = 6.82(3)4% for 10 K.

The XRD results are shown in Fig. 2. The diffraction patterns were processed by Rietveld refinement[47] in the program TOPAS.[48] The XRD measurements performed on the sample annealed at 1273 K related to approximately 70% (weight %) of the $EuTiO_3$ phase, with a lattice parameter a = 3.910 Å. A secondary phase, Ti_3O_5, precipitated in the sample structure, probably as a consequence of annealing in vacuum, where the oxygen partial pressure was not controlled. Around 30% of the Ti_3O_5 presented lattice parameters of a = 9.98 Å, b = 5.08 Å, c = 7.16 Å, and β = 109.91. It is important to emphasize that the Ti_3O_5 phase was not observed in the TDPAC experiments.

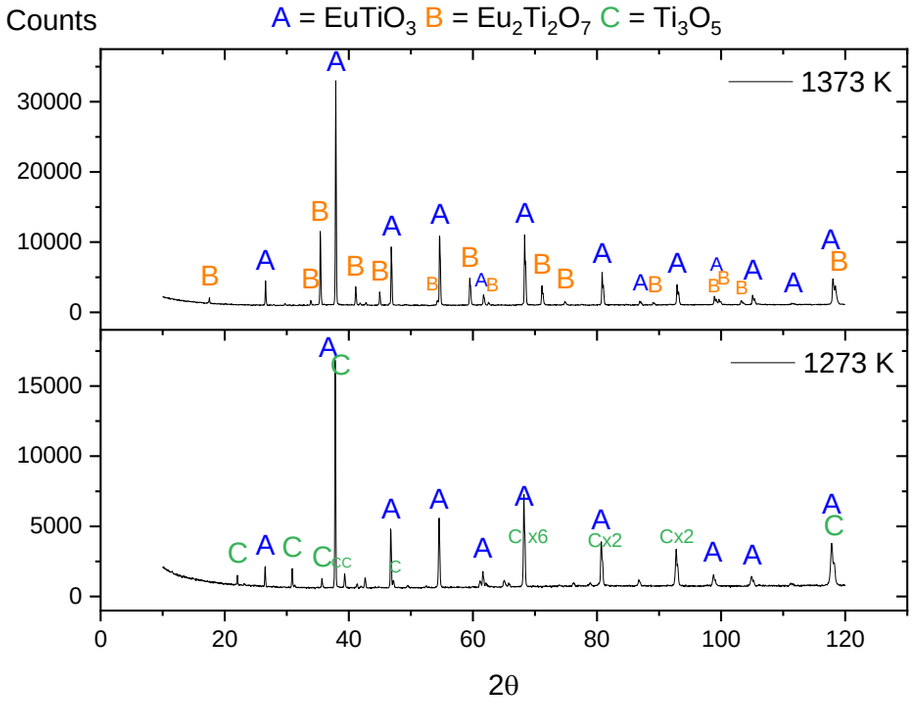

FIG. 2. X-ray diffractogram of the samples performed following annealing at 1373 K (top) and 1273 K (bottom). For better visualization, the main peaks of the phases have been designated A, B, and C.

For the samples annealed at 1373 K, the XRD measurements showed approximately 72% (weight %) of the $EuTiO_3$ phase with a lattice parameter a = 3.905 Å and around 28% of $Eu_2Ti_2O_7$ with a = 10.212 Å. The lattice parameters of $EuTiO_3$ were relatively high, being evidence of point defects.[49]

Evidence for vacancy trapping associated with a change in the Eu charge-state (from 2+ to 3+) was found following annealing at 1373 K, as shown in Fig. 1 (right); a static V_{zz} of approximately 22×10^{21} V/m^2 with $\eta = 0$ and a well-defined quadrupole frequency at 10 K and RT could be observed for site (local environment) 1. This static interaction arises from a specific Eu charge state and defect configuration to which the Ta probe attaches.

Europium is the most volatile metal of the lanthanide series. During all high-temperature treatments of the $EuTiO_3$ samples (and mainly in a vacuum because of low partial pressures), small amounts of Eu were evaporated, disrupting the stoichiometry of the perovskite structure ($Eu_{1-x}TiO_{3-y}$) to a small degree. This metastable composition began to decompose during annealing in the vacuum.

Table I gives the corresponding experimental hyperfine parameters for the experiments following annealing at 1373 K with Gaussian distributions. The observed quadrupole interaction frequency for site 1 decreased with increasing temperature. This behavior can be assigned to the general increase in the bond lengths resulting from thermal expansion of the crystal lattice, thereby reducing the nuclear quadrupole interaction. To obtain the experimental V_{zz} value, the Q = 2.28(2) b value[50,51] was considered, leading to a V_{zz} error of approximately 10%. In addition to the high Q value, the probe ^{181}Hf has several properties, which make it a very convenient isotope for TDPAC experiments. It has a long half-life of 42.4 days and it decays over β^- to an excited state of Ta.[51] The TDPAC measurement is performed using the 133–482 keV cascade with the intermediate I = 5/2 state, which has a half-life of 10.6 ns and +3.29(3) μ_N.[51]

TABLE I. Experimental hyperfine parameters for the different measuring temperatures following annealing at 1373 K.

T (K)	V_{zz} (10^{21} V/m^2)	η	δ (%)	Fraction (%)	Fixed $\langle\omega_0\rangle$ (Mrad/s)	η	FWHM (%)	Fraction (%)

10	22.4	0.12(1)	6.7(2)	75.0(5)	1	0	6.82(3)	25.0(3)
295	21.5	0.07(1)	7.2(5)	77.2(6)	1	0	1.27(1)	22.8(2)
	site 1				site 2			

The EFG distribution FWHM and fraction for site 2 decreased with increasing measurement temperature. In order to correlate the extracted hyperfine parameters with the location of the probe nuclei ($^{181}Ta^{5+}$) at ionic sites in $EuTiO_3$, *ab initio* calculations were carried out as follows:

With a cubic $Pm\bar{3}m$ structure, V_{zz} was shown to be zero for Ta that was simply substitutional at the Eu or Ti sites, due to symmetry. We then considered the case of an oxygen vacancy (Ov) as nearest neighbor (nn) to Ta substitutional at Ti or Eu sites, starting with a $2 \times 2 \times 2$ supercell. For Ta, substitutional at the Ti site with an nn Ov, we obtained $V_{zz} = 31.80 \times 10^{21}$ V/m^2 for G-AFM order. Calculations with GGA + U (GGA) predicted $V_{zz} = 34.4 \times 10^{21}$ V/m^2 (33.24 for GGA) and $\eta = 0.16$ (0.31 for GGA). We used GGA + U, as it was probably the better approximation, for the remaining calculations. (We tested the effect of different lattice parameters: using $a = 3.85$ and 3.95 Å resulted in $V_{zz} = 37.4 \times 10^{21}$ V/m^2, $\eta = 0.22$, and $V_{zz} = 32.2 \times 10^{21}$ V/m^2, $\eta = 0.14$, respectively.) However, this supercell was small, and we performed calculations with $3 \times 3 \times 3$ and $4 \times 4 \times 4$ supercells to remove any possible effects from interactions between the periodic defects (since the calculations were periodic, any defect would not have been disordered, as in a real sample, and may have interacted with its images if the supercell had not been large enough). The results, $V_{zz} = 46.6 \times 10^{21}$ V/m^2 ($3 \times 3 \times 3$) and 45.9×10^{21} V/m^2 ($4 \times 4 \times 4$), showed convergence with supercell size, but were even higher and compared worse with the experimental low-temperature values. We also performed calculations with a next-nearest neighbor (nnn) Ov.

Ta that is substitutional at the Eu site with one nn Ov resulted in $V_{zz} \sim 71 \times 10^{21}$ V/m^2, $\eta = 0.44$, which is also far from the experimental value. The result with an nnn Ov decreased to a lower value of $V_{zz} \sim 56 \times 10^{21}$ V/m^2, but was still much higher than the experimental value, also with higher η, and was energetically unfavorable with respect to the nn case by 143 meV/fu. These results indicate that in the cubic phase the experimental data cannot be explained by the Ta substitutional probe at the Ti or Eu sites, including cases with an Ov near the substitutionalsites (Ta:Ti and Ta:Eu). The results are summarized in Table II.

TABLE II. Simulated values for *Pm-3m* with oxygen vacancies (Ov).

Site	Supercell	V_{zz} (10^{21} V/m^2)	η
Ta:Ti with nn Ov	2 × 2 × 2	36.3	0.00
Ta:Ti with nn Ov	3 × 3 × 3	46.6	0.00
Ta:Ti with nn Ov	4 × 4 × 4	45.9	0.00
Ta:Eu with nn Ov	2 × 2 × 2	70.7	0.44
Ta:Eu with nnn Ov	2 × 2 × 2	56.5	0.75

Next, we explored several other structures that have been studied and proposed for this material,[44] with *I4/mcm*, *Imma,* and $R\bar{3}c$ space groups, which exhibits rotations of oxygen octahedra. Starting with these initial structures, we then included defects, which produced an additional decrease in symmetry. With these structures, the EFG with Ta at substitutional sites is not zero, but is small (except for high concentrations of Ta:Eu starting with the *I4/mcm* space group). The results for Ta in different supercells of the different phases are given in Tables III–V. For Ta at Ti sites, the variation is small between phases (0 in the cubic phase to −3 in the *I4/mcm* space group), which indicates that in all cases, a simple substitutional Ti situation was not measured. With Ta at Eu, it is notable that the EFG changes drastically from the 1 × 1 × 1 supercell to the 2 × 2 × 1 supercell in the *I4/mcm* phase, though none of these calculations are consistent with experimental results. The low values obtained in simple substitutions with low Ta concentrations indicate that other defects must be considered. Oxygen vacancies may of course greatly change the results seen in the cubic phase, so we also considered Ov in the *I4/mcm* and *Imma* phases. Finally, Ta, substitutional at Eu and with an nn Ov, agrees with the experimental value (V_{zz} = 22 x 10^{21} V/m^2). The value is also close to, but less than, the experimental one if we consider the same kind of defect from the *I4/mcm* phase, with V_{zz} = 17.9 x 10^{21} V/m^2. To complete the set of proposed structures with octahedral rotations, we also considered the $R\bar{3}c$ space group (here the oxygen octahedra have the same alternating rotation angles in all three directions, corresponding to the a$^-$a$^-$a$^-$ rotation pattern in Glazer's notation).[52] In addition, we considered 2 × 2 × 1 supercells with respect to the hexagonal unit cell (separations of 11.06 Å between Ta impurities; one calculation with a 1 × 1 × 1 supercell revealed a small difference in electric field gradient, V_{zz} = 2.0 x 10^{21} V/m^2), resulting in V_{zz} = 2.1 x 10^{21} V/m^2 and 48.2 x 10^{21} V/m^2 for Ti and Eu substitutions, respectively, neither of which is close to the experimental value. The results are summarized in Table III.

TABLE III. Simulated values for different crystal symmetries in $EuTiO_3$.

I4/mcm

Site	Supercell	V_{zz} (10^{21} V/m^2)	η
Ta:Ti	1 × 1 × 1	−3.3	0.05
Ta:Ti	2 × 2 × 1	0.6	0.05
Ta:Eu	1 × 1 × 1	−39.5	0
Ta:Eu	2 × 2 × 1	−1.8	0
Ta:Eu with nn Ov	2 × 2 × 1	17.9	0.68

Imma

Site	Supercell	V_{zz} (10^{21} V/m^2)	η
Ta:Ti	1 × 1 × 1	−2.4	0.22
Ta:Ti	2 × 1 × 2	−2.8	0.63
Ta:Ti with nn Ov	2 × 1 × 2	41.1	0.05
Ta:Eu	1 × 1 × 1	−7.5	0.63
Ta:Eu	2 × 1 × 2	−7.6	0.90
Ta:Eu with nn Ov	2 × 1 × 2	22.1	0.69

R-3c

Site	Supercell	V_{zz} (10^{21} V/m^2)	η
Ta:Ti	1 × 1 × 1	2.0	0.00
Ta:Ti	2 × 2 × 1	2.1	0.00
Ta:Eu	2 × 2 × 1	48.2	0.00

To check the possibility of a pyrochlore phase, (*Fd-3m*) $Eu_2Ti_2O_7$, we performed calculations with Ta substitutional at Eu and Ti sites. Since one unit cell of $Eu_2Ti_2O_7$ already contained eight formula units (one formula unit contained the same atoms as the chemical formula, $Eu_2Ti_2O_7$), we did not increase cell size in this case. The results are presented in Table IV. The existence of this phase was confirmed by our XRD and TDPAC results, following annealing at 1373 K. The experimental parameters ($V_{zz} \approx 22 \times 10^{21}$ V/m^2 with $\eta \approx 0.1$) were close to the simulated values. This is a more realistic result, in contrast with the calculation for $EuTiO_3$ with *Imma* symmetry and Ta at the Eu site with an Ov ($V_{zz} = 22.1 \times 10^{21}$ V/m^2 with $\eta = 0.69$). The reason, we expect, is that Ta occupies the Ti site and the configuration of its Eu site with an Ov is energetically unfavorable. Furthermore, the $Eu_2Ti_2O_7$ phase was also observed in the XRD results, and the simulated asymmetry parameter agrees with the experimental one.

TABLE IV. Simulated values for $Eu_2Ti_2O_7$.

Site	V_{zz} (10^{21} V/m^2)	H
Ta:Ti	18.4	0
Ta:Eu	−57.3	0

Regarding the Ti_3O_5 phase, the lattice parameters measured by XRD were considered, and for the calculation, we used a $1 \times 2 \times 2$ supercell. The calculations used GGA + U (U = 5.7, J = 1 eV for Eu f electrons), a $4 \times 3 \times 3$ k-points grid, an energy cutoff of 500 eV, and a spin-polarized ferromagnetic solution was considered [final moments at Ti were of the order of 0.2–0.4 μ_B, while Ta had a small moment of 0.05 μ_B; O atoms had very small negative moments (~ -0.01 μ_B)]. The results of the EFG contribution are presented in Table V where the calculation with and without minus one electron give very similar results. The Ti_3O_5 phase was not observed in the TDPAC experiments, but was discovered in XRD. A possible explanation is that the Ti_3O_5 phase was not present in the neighborhood of the TDPAC probe. The local environment of the probes is subjected to the implantation range and thermal diffusion range during thermal annealing and high temperature experiments. In our case, implantation was performed in a 3 mm x 3 mm area and with a very low concentration of the ^{181}Ta probe.

TABLE V. Simulated values for Ti_3O_5.

Site	V_{zz} (10^{21} V/m^2)	η
Ta:Ti	8.4	0.76
Ta:Ti with minus one electron	8.4	0.79

An actual measurement of the limit for the electron electric dipole moment (EDM) with $Eu_{0.5}Ba_{0.5}TiO_3$ was reported by Eckel *et al.*.[53] This type of measurement has not been further pursued because other measurement methods today show greater promise. The principal advantage of this solid-state method resides in the fact that one can easily upscale sample production and gain immediately EDM thanks to statistical analysis, which is not so easy with neutron or radium EDM measurements. To date, the TDPAC technique has not been used to determine the EDM.

Our results demonstrate the feasibility of using the TDPAC technique to study hyperfine interactions in $EuTiO_3$, complemented by *ab initio* calculations and XRD experiments. The comparison with ab-initio calculations allows one to assign the Ti site in the $Eu_2Ti_2O_7$ phase

the most probable site for Ta probes. The calculations further show that using the EFG is one way to discriminate between different possible structures, sites, and point defects in $EuTiO_3$ using TDPAC with Ta probes.

The variety of unusual and interesting ferroelectric, magnetic, and structural properties in europium titanates requires such local characterization for a deeper understanding of the Eu^{3+}/Eu^{2+} influence. The observed static interaction arises from a specific Eu charge state and defect configuration to which the Ta probe attaches. Point defects combined with Eu ions strongly influence the temperature of the phase transitions, and a proper configuration can achieve considerable magnetic susceptibility and strong spin-orbit and/or spin-phonon coupling. The TDPAC technique is well known in the investigation of point defects. Depending on the preparation method used for incorporating the radioactive probe atoms, it is possible to study the material without changing its properties. In this case, interference of the probe atoms with the properties of the sample and doping levels can be excluded.[54] Additional TDPAC measurements with $EuTiO_3$ are foreseen and are part of the ISOLDE-CERN project IS647 "Local Probing of Ferroic and Multiferroic Compounds".[55,56,57]

IV. CONCLUSIONS

The main intention of this work was to study the electric-field gradient at the Ti and Eu sites in europium titanates by means of perturbed angular correlations, XRD diffraction, and *ab initio* calculations. We conclude that annealing at 1373 K changes the charge state of Eu, being related to the partial phase transition to the $Eu_2Ti_2O_7$ phase. Moreover, the $Eu_2Ti_2O_7$ phase was also observed in the XRD experiments, and the simulated parameters for Ta at the Ti site ($V_{zz} = 18.4 \times 10^{21}$ V/m^2 with $\eta = 0$) are close to the experimental ones ($V_{zz} \approx 22 \times 10^{21}$ V/m^2 with $\eta \approx 0.1$). Such annealing effects in $EuTiO_3$ and $Eu_2Ti_2O_7$ have not been studied, to our knowledge, until now by means of perturbed angular correlations. The TDPAC results are in agreement with those of *ab initio* calculations and XRD diffraction, confirming the existence of the $EuTiO_3$ and $Eu_2Ti_2O_7$ phases. However, the Ti_3O_5 phase was not observed in the TDPAC experiments. The structural phase transition from cubic to tetragonal, which should occur between 282 and 300 K, was not observed, since measurements were carried out at temperatures of up to 295 K only. The induction of additional phases, $Eu_2Ti_2O_7$ and Ti_3O_5, during the annealing process was complemental to the study of pure $EuTiO_3$.

ACKNOWLEDGMENTS

The research leading to these results has received funding from the Federal Ministry of Education and Research (BMBF) through Grant 05K16PGA. The authors also acknowledge the support of the Czech Science Foundation (Projects Nos. 18-09265S and 17-05620S) and support from the Ministry of Education, Youth and Sports of the Czech Republic under Projects CEITEC 2020 (LQ1601) and SOLID21 (CZ.02.1.01/0.0/0.0/16_019/0000760). We also acknowledge support from the Portuguese Foundation for Science and Technology (FCT) under Project CERN-FIS-NUC-0004-2015. The Danish Ministry of Higher Education and Science is thanked for financial support via the NICE grant. We thank J. G. M. Correia for technical assistance during these experiments and U. Koester for the irradiation at the Institut Laue-Langevin. We also thank V. V. Shvartsman for fruitful discussions.

The authors declare no competing interests.

[1]J. Schell, P. Schaaf, and D. C. Lupascu, AIP Adv. **7**, 105017 (2017).

[2]G. Schäfer, P. Herzog, and B. Wolbeck, Z. Phys. **257**, 336 (1972).

[3]Gary L. Catchen, Edward F. Hollinger, and Todd M. Rearick, Z. Naturforsch. A **51**, 411 (1996).

[4]J. N. Gonçalves, A. Stroppa, J. G. Correia, T. Butz, S. Picozzi, A. S. Fenta, and V. S. Amaral, Phys. Rev. B **86**, 035145 (2012).

[5]P. Chandra and P. B. Littlewood, Physics of Ferroelectrics: A Modern Perspective, Topics in Applied Physics **105**, 69, (2007).

[6]D. Bessas, K. Z. Rushchanskii, M. Kachlik, S. Disch, O. Gourdon, J. Bednarcik, K. Maca, I. Sergueev, S. Kamba, M. Ležaić, and R. P. Hermann, Phys. Rev. B **88**, 144308 (2013).

[7]Y. Zong, K. Kugimiya, K. Fujita, H. Akamatsu, K. Hirao, and K. Tanaka, J. Non-Cryst. Solids **356**, 2389 (2010).

[8]H. Akamatsu, K. Fujita, H. Hayashi, T. Kawamoto, Y. Kumagai, Y. Zong, K. Iwata, F. Oba, I. Tanaka, and K. Tanaka, Inorg. Chem. **51**, 4560 (2012).

[9]C.-L. Chien, S. DeBenedetti, and F. De S. Barros, Phys. Rev. B **10**, 3913 (1974).

[10]O. Berkooz, J. Phys. Chem. Solids **30**, 1763(1969).

[11]K. Z. Rushchanskii, S. Kamba, V. Goian, P. Vaněk, M. Savinov, J. Prokleška, D. Nuzhnyy, K. Knížek, F. Laufek, S. Eckel, S. K. Lamoreaux, A. O. Sushkov, M. Ležaic, and N. A. Spaldin, Nat. Mater. **9**, 649 (2010).

[12]T. Katsufuji, and H. Takagi, Phys. Rev. B **64**, 054415 (2001).

[13]J. H. Lee, L. Fang, E. Vlahos, X. Ke, Y. W. Jung, L. Fitting Kourkoutis, J.-W. Kim, P. J. Ryan, T. Heeg, M. Roeckerath, V. Goian, M. Bernhagen, R. Uecker, P. Ch. Hammel, K. M. Rabe, S. Kamba, J. Schubert, J. W. Freeland, D. A. Muller, C. J. Fennie, P. E. Schiffer, V. Gopalan, E. Johnston-Halperin, and D. G. Schlom, Nature **466**, 954 (2010).

[14]V. V. Shvartsman, P. Borisov, W. Kleemann, S. Kamba, and T. Katsufuji, Phys. Rev. B **81**, 064426 (2010).

[15]A. Bussmann-Holder, J. Köhler, R. K. Kremer, and J. M. Law, Phys. Rev. B **83**, 212102 (2011).

[16]V. Goian, S. Kamba, O. Pacherová, J. Drahokoupil, L. Palatinus, M. Dušek, J. Rohlíček, M. Savinov, F. Laufek, W. Schranz, A. Fuith, M. Kachlík, K. Maca, A. Shkabko, L. Sagarna, A. Weidenkaff, and A. A. Belik, Phys. Rev. B **86**, 054112 (2012).

[17]J. Köhler, R. Dinnebier, and A. Bussmann-Holder, Phase Transit. **85**, 949 (2012).

[18]A. Pal, A. Singh, A. K. Ghosh, and S. Chatterjee, J. Magn. Magn. Mater **462**, 1 (2018).

[19]J. Mrázek, M. Surýnek, S. Bakardjieva, J. Buršík, J. Proboštová, and I. Kašík, J. Alloys Compd **645**, 57 (2015).

[20]A. F. Arif, R. Balgis, T. Ogi, F. Iskandar, A. Kinoshita, K. Nakamura, and K. Okuyama, Sci. Rep. **7**, 3646 (2017).

[21]M. Kachlik, K. Maca, V. Goian, and S. Kamba, Mater. Lett. **74**, 16 (2012).

[22]K. Freitag, Radiation Effects **44**, 185 (1979).

[23]J. Schell, D. C. Lupascu, A. W. Carbonari, R. D. Mansano, I. S. Ribeiro Jr., T. T. Dang, I. Anusca, H. Trivedi, K. Johnston, and R. Vianden, J. Appl. Phys. **121**, 145302 (2017).

[24]K. Johnston, J. Schell, J. G. Correia, M. Deicher, H. P. Gunnlaugsson, A. S. Fenta, E. David-Bosne, A. R. G. Costa, and D. C. Lupascu, J. Phys. G **44**, 104001 (2017).

[25]M. J. G. Borge, and B. Jonson, J. Phys. G **44**, 044011 (2017).

[26]T. Butz, S. Saibene, T. H. Fraenzke, and M. Weber, Nucl. Instrum. Methods Phys. Res. A **284**, 417 (1989).

[27]M. Nagl, U. Vetter, M. Uhrmacher, and H. Hofsäss, Rev. Sci. Instrum. **81**, 073501 (2010).

[28]Nightmare (MDI) Version RC 3 (1.2.0.247). Copyright (2005–2010) from the group Reiner Vianden and (2008–2010) Ronan Nédélec, Bonn University, Germany.

[29]T. Butz, Hyperfine Interact**. 52**, 189 (1989).

[30]A. Abragam, and R. V. Pound, Phys. Rev. **92**, 943 (1953).

[31]H. Frauenfelder, R. M. Steffen, and K. Siegbahn. *α-, β- and γ-Ray Spectroscopy*, edited by K. Siegbahn, North-Holland, Amsterdam (1965).

[32]H. Jaeger, L. Abu-Raddad, and D. J. Wick, Appl. Radiat. Isot. **48**, 1083 (1997).

[33]T. T. Dang, J. Schell, D. C. Lupascu, and R. Vianden, J. Appl. Phys. **123**, 165109 (2018).

[34]R. Vianden, and U. Feuser, Phys. Rev. Lett. **61**, 1981 (1988).

[35]S. M. van Eek, and M. Forker, Phys. Rev. B **65**, 174307 (2002).

[36]D. Lupascu, S. Habenicht, K. P. Lieb, M. Neubauer, M. Uhrmacher, and T. Wenzel, Phys. Rev. B **54**, 871 (1996).

[37]J. Schell, D. C. Lupascu, J. G. M. Correia, A. W. Carbonari, M. Deicher, M. B. Barbosa, R. D. Mansano, K. Johnston, I. S. Ribeiro Jr., and ISOLDE collaboration, Hyperfine Interact. **238**, 2 (2016).

[38]G. K. Wertheim, M. A. Butler, K. W. West, and D. N. E. Buchanan, Rev. Sci. Instrum. **45**, 1369 (1974).

[39]J. G. Martins Correia, ISOLDE-CERN, private communication (2018).

[40]J. Christiansen, P. Heubes, R. Keitel, W. Klinger, W. Loeffler, W. Sandner, and W. Witthuhn, Z. Phys. B **24**, 177 (1976).

[41]P. E. Blöchl, Phys. Rev. B **50**, 17953 (1994).

[42]G. Kresse, and J. Furthmüller, Phys. Rev. B **54**, 11169 (1996).

[43]J. P. Perdew, K. Burke, and M. Ernzerhof, Phys. Rev. Lett. **77**, 3865 (1996).

[44]K. Z. Rushchanskii, N. A. Spaldin, and M. Ležaić, Phys. Rev. B **85**, 104109 (2012).

[45]J. Lee, L. Fang, E. Vlahos, X. Ke, Y. W. Jung, L. F. Kourkoutis, J. W. Kim, P. J. Ryan, T. Heeq, M. Roeckerath, V. Goian, M. Bernhagen, R. Uecker, P. C. Hammel, K. M. Rabe, S. Kamba, J. Schubert, J. W. Freeland, D. A. Muller, C. J. Fennie, P. Schiffer, V. Gopalan, E. Johnston-Halperin, and D. G. Schlom, Nature **466**, 954 (2010).

[46]S. L. Dudarev, G. A. Botton, S. Y. Savrasov, C. J. Humphreys, and A. P. Sutton, Phys. Rev. B **57**, 1505 (1998).

[47]H. M. Rietveld, J. Appl. Crystallogr. **2**, 65, (1969).

[48]R.W. Cheary, A. A. Coelho, and J. P. Cline, J. Res. Natl. Inst. Stand. Technol. **109**, 1 (2004).

[49]W. Gong, H. Yun, Y. B. Ning, J. E. Greedan, W. R. Datars, and C. V. Stager, J. Solid State Chem. **90**, 320 (1991).

[50]N. J. Stone, At. Data Nucl. Data Tables **111**, 1 (2016).

[51]A. Jancso, J. Correia, A. Gottberg, J. Schell, M. Stachura, D. Szunyogh, S. Pallada, D. Lupascu, M. Kowalska, and L. Hemmingsen, J. Phys. G **44**, 064003 (2017).

[52]A. M. Glazer, Acta Cryst. B **28**, 3384 (1972).

[53]S. Eckel, A. O. Sushkov, and S. K. Lamoreaux, Phys. Rev. Lett. **109**, 193003 (2012).

[54]T. Wichert, and E. Recknagel in *Microscopic Methods in Metals*, Topics in Current Physics, Vol. 40, p. 317, edited by U. Gonser (Springer-Verlag, Heidelberg, New York, 1986).

[55]A. M. L. Lopes, J. Schell, V. S. Amaral, C.O. Amorim, J. P. Araújo, A. Baghizadeh, M. Baptista, H.-W. Becker, M. E. Castillo, J. G. Correia, A. Fenta, J. N. Gonçalves, H. Haas, M. Kachlik, S. Kamba, A. L. Kholkin, A. A. Lourenço, D. C. Lupascu, K. Maca, G. Oliveira, S. Picozzi, A. L. Pires, E. C. Queirós, P. Rocha-Rodrigues, V. Shvartsman, M. R. Silva, A. Stroppa, P. B. Tavares, J. M. Vieira, and Y. Vysochanskii, P-502-Local Probing Of Ferroic And Multiferroic Compounds, ISOLDE-CERN active experiment IS647 (2017).

[56]J. Schell, H. Hofsäss, and D. C. Lupascu, Using radioactive beams to unravel local phenomena in ferroic and multiferroic materials, Nucl. Instrum. Methods Phys. Res. B. **XX**, XXX Just accepted https://doi.org/10.1016/j.nimb.2019.06.016

[57] J. Schell and G. Marschick, "TDPAC Studies of Local Defects and Phenomena in Ferroics and Multiferroics", Crystals 9(12) (2019) 611, https://doi.org/10.3390/cryst9120611

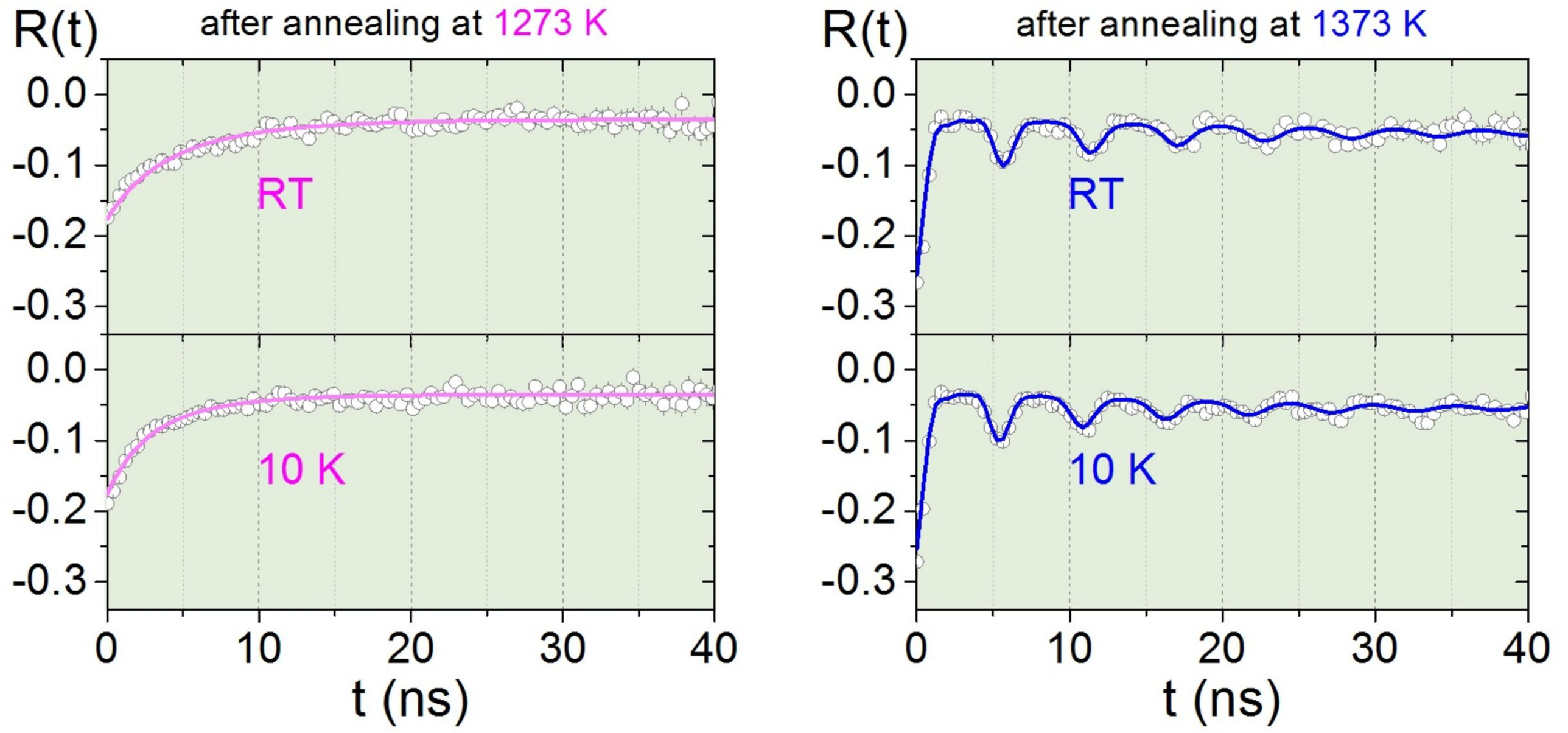
R(t)
after annealing at 1273 K
RT
10 K
0.0
-0.1
-0.2
-0.3
0
10
20
30
40
t (ns)
R(t)
after annealing at 1373 K
RT
10 K
0.0
-0.1
-0.2
-0.3
0
10
20
30
40
t (ns)

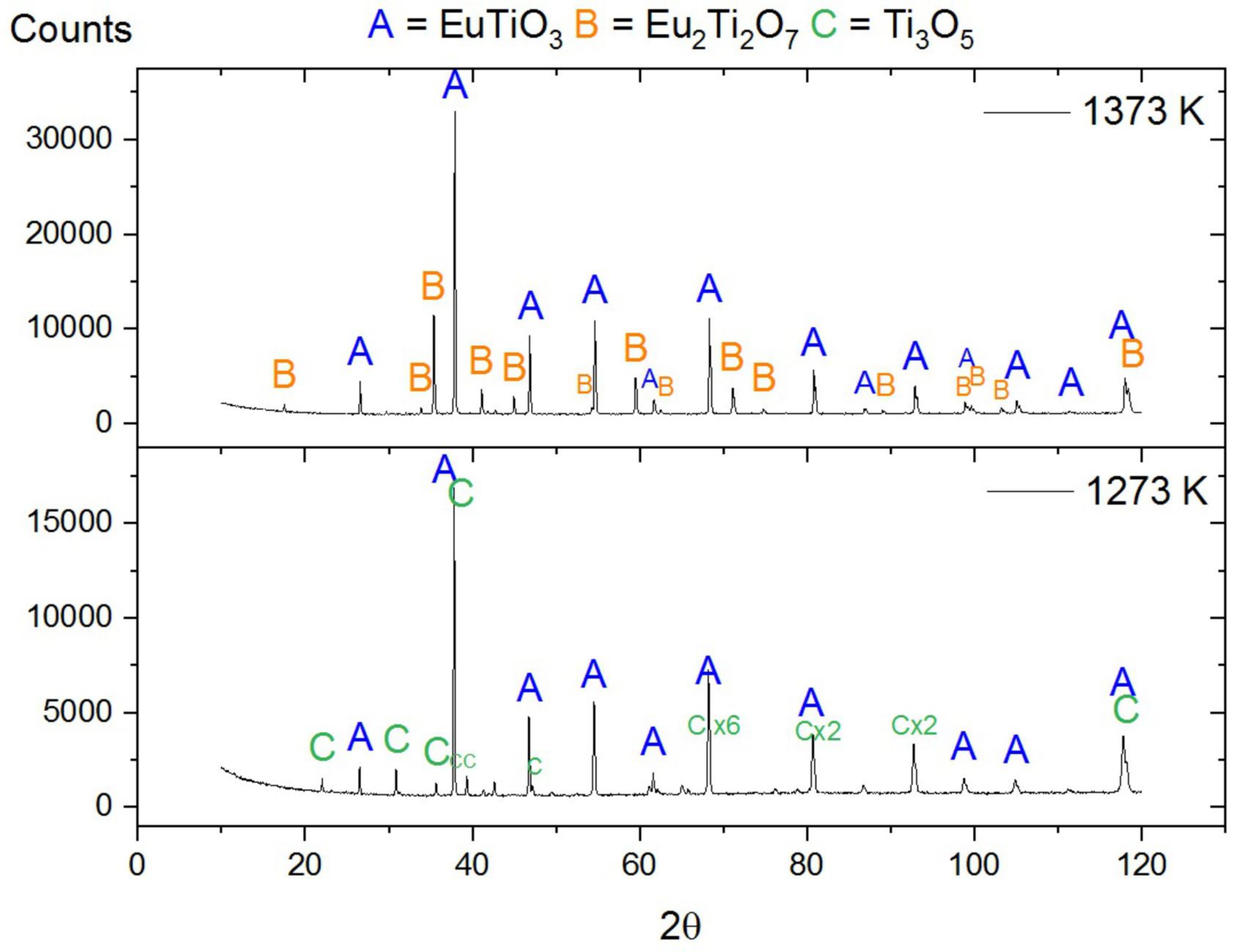
Counts
A = EuTiO3 B = Eu2Ti2O7 C = Ti3O5
1373 K
1273 K
30000
20000
10000
0
15000
10000
5000
0
0
20
40
60
80
100
120
2θ
Cx6
Cx2
Cx2